Available online at www.sciencedirect.com
SCIENCE DIRECT®
Journal of Computational Physics 202 (2005) 196–215
JOURNAL OF COMPUTATIONAL PHYSICS
www.elsevier.com/locate/jcp

ADER schemes for scalar non-linear hyperbolic conservation laws with source terms in three-space dimensions

E.F. Toro [a], V.A. Titarev [b,*]

[a] *Laboratory of Applied Mathematics, Faculty of Engineering, University of Trento, Trento, Italy*
[b] *Department of Mathematics, Faculty of Science, University of Trento, Trento, 38080 Povo, Italy*

Received 13 October 2003; received in revised form 3 June 2004; accepted 22 June 2004
Available online 13 August 2004

Abstract

In this paper we develop non-linear ADER schemes for time-dependent scalar linear and non-linear conservation laws in one-, two- and three-space dimensions. Numerical results of schemes of up to fifth order of accuracy in *both time and space* illustrate that the designed order of accuracy is achieved in all space dimensions for a fixed Courant number and essentially non-oscillatory results are obtained for solutions with discontinuities. We also present preliminary results for two-dimensional non-linear systems.

Keywords: High-order schemes; Weighted essentially non-oscillatory; ADER; Generalized Riemann problem; Three-space dimensions

1. Introduction

This paper is concerned with the construction of non-linear schemes of the ADER type for time-dependent scalar linear and non-linear conservation laws in one-, two- and three-space dimensions. The ADER approach was first put forward by Toro and collaborators [25], where the idea was illustrated for solving the linear advection equation with constant coefficients. Formulations were given for one, two and three-dimensional *linear* schemes on regular meshes and implementation of *linear* schemes of up to 10th order in space and time for both the one-dimensional and the two-dimensional case were reported. We also mention the work of Schwartzkopff et al. [14,15], where linear schemes of upto sixth order in space and time were

* Corresponding author.
E-mail addresses: toro@ing.unitn.it (E.F. Toro), titarev@science.unitn.it (V.A. Titarev).
URLs: http://www.ing.unitn.it/torohttp://www.science.unitn.it/~titarev

0021-9991/$ - see front matter
doi:10.1016/j.jcp.2004.06.014

constructed. These were then applied to acoustic problems and detailed comparison with other schemes was carried out.

The extension of the ADER approach to non-linear problems relies on the solution of the generalised Riemann problem. For non-linear systems, including source terms, this was presented in [26]. Construction of ADER schemes for the one-dimensional Euler equations using this Riemann problem solution has been reported in [19,27]. For the construction of schemes as applied to non-linear scalar equations in one-space dimension see also [18]. Extension of ADER to scalar advection–diffusion–reaction equations in one-space dimension is reported in [20], where explicit non-linear schemes of up to sixth order are presented.

As is well known from the theorem of Godunov [5], high-order *linear* schemes will generate spurious oscillations near discontinuities or sharp gradients of the solution. These oscillations pollute the numerical solution and are thus highly undesirable. To avoid generating spurious oscillations, non-linear solution-adaptive schemes must be constructed. It appears as if it was Kolgan [10] who first proposed to suppress spurious oscillations by applying the so-called principle of minimal values of derivatives, producing in this manner a non-oscillatory (TVD) Godunov-type scheme of second-order spatial accuracy. Further, more well-known, developments are due to van Leer [28,29]. In multiple-space dimensions unsplit second-order non-oscillatory methods were constructed by Kolgan [11], Tiliaeva [17], Colella [4] and many others. Uniformly high-order extensions of these methods are represented by essentially non-oscillatory (ENO) [8,2] and weighted essentially non-oscillatory (WENO) [12,7,1,9,16] schemes.

In one-space dimension non-linear (non-oscillatory) ADER schemes of up to fifth order of accuracy in time and space have been presented in [25,19,27,18]. In two-space dimensions, however, the ADER approach has so far been limited to linear schemes and linear equations only [25,14,15] and therefore cannot be used as such for computing discontinuous solutions. However, we are aware of work in progress by Kaeser (private communication) for the two dimensional non-linear scalar case. We also remark that no three-dimensional ADER schemes, either linear or non-linear, have yet been presented.

The motivation of this paper is threefold. First, we carry out the construction of *non-linear* ADER schemes in two- and three-space dimensions. These schemes generalize linear two-dimensional ADER schemes developed [25,14,15]. Second, we extend the ADER approach to non-linear scalar conservation laws with reactive-like source terms in two- and three-space dimensions thus extending non-linear one-dimensional ADER schemes of [19,27,18,20] to multiple-space dimensions.

We present numerical examples for schemes of up to fifth order of accuracy in *both time and space*, which illustrate that the schemes indeed retain the designed order of accuracy in all space dimensions and produce essentially non-oscillatory results for solutions with discontinuities. This should be compared with the state-of-the art weighted essentially non-oscillatory (WENO) schemes [7,1,16] and Runge–Kutta discontinuous Galerkin finite element methods [3], which generally achieve only third order of time accuracy if *non-linear*, *non-oscillatory* methods are to be used.

Finally, we include some preliminary results on the extension of the method to non-linear two-dimensional systems of conservation laws.

The rest of the paper is organized as follows. In Section 2 we review the ADER approach in one-space dimension as applied to advection–reaction equations. Extension to three-space dimensions is carried out in Section 3. Numerical examples are provided in Section 4. In Section 5 we present preliminary results on the extension of the method to non-linear multidimensional systems. Conclusions are drawn in Section 5.

2. Review of ADER schemes in one-space dimension

Consider the following one-dimensional nonlinear advection–reaction equation:

$$\partial_t q + \partial_x f(q) = s(x,t,q), \tag{1}$$

where $q(x,t)$ is the unknown conservative variable, $f(q)$ is the physical flux and $s(x,t,q)$ is a source term. Integration of (1) over the control volume in x–t space $I_i \times \Delta t$, $I_i = [x_{i-1/2}, x_{i+1/2}]$, of dimensions $\Delta x = x_{i+1/2} - x_{i-1/2}$, $\Delta t = t^{n+1} - t^n$, gives

$$q_i^{n+1} = q_i^n + \frac{\Delta t}{\Delta x}\left(f_{i-1/2} - f_{i+1/2}\right) + \Delta t\, s_i, \tag{2}$$

where q_i^n is the cell average of the solution at time level t^n, $f_{i+1/2}$ is the time average of the physical flux at cell interface $x_{i+1/2}$ and s_i is the time–space average of the source term over the control volume:

$$\begin{aligned} q_i^n &= \frac{1}{\Delta x}\int_{x_{i-1/2}}^{x_{i+1/2}} q(x,t^n)\,\mathrm{d}x, \quad f_{i+1/2} = \frac{1}{\Delta t}\int_{t^n}^{t^{n+1}} f(q(x_{i+1/2},\tau))\,\mathrm{d}\tau, \\ s_i &= \frac{1}{\Delta t}\frac{1}{\Delta x}\int_{t^n}^{t^{n+1}}\int_{x_{i-1/2}}^{x_{i+1/2}} s(x,\tau,q(x,\tau))\,\mathrm{d}x\,\mathrm{d}\tau. \end{aligned} \tag{3}$$

Eq. (2) involving the integral averages (3) is upto this point an exact relation, but can be used to construct numerical methods to compute approximate solutions to (1). This is done by subdividing the domain of interest into many disjoint control volumes and by defining approximations to the flux integrals, called numerical fluxes, and to the source integral, called numerical source. Let us denote the approximations to these integrals by the same symbols $f_{i+1/2}$ and s_i in (3). Then formula (2) is a conservative one-step scheme to solve (1).

The ADER approach defines numerical fluxes and numerical sources in such a way that the explicit conservative one-step formula (2) computes numerical solutions to (1) to arbitrarily high order of accuracy in both space and time. The approach consists of three steps: (i) reconstruction of pointwise values from cell averages, (ii) solution of a generalized Riemann problem at the cell interface and evaluation of the intercell flux $f_{i+1/2}$ and (iii) evaluation of the numerical source term s_i by integrating a time–space Taylor expansion of the solution inside the cell.

The pointwise values of the solution at $t = t^n$ are reconstructed from cell averages by means of high-order polynomials. To avoid spurious oscillations ENO [8] or WENO [12,7] reconstruction can be used, leading to *non-linear* schemes. In general, WENO reconstruction produces more accurate results and therefore it is used in the design of our schemes. By means of the reconstruction step the conservative variable is represented by polynomials $p_i(x)$ in each cell I_i. At each cell interface we then have the following generalized Riemann problem:

$$\begin{aligned} &\partial_t q + \partial_x f(q) = s(x,t,q), \\ &q(x,0) = \begin{cases} q_{\mathrm{L}}(x) = p_i(x), & x < x_{i+1/2}, \\ q_{\mathrm{R}}(x) = p_{i+1}(x), & x > x_{i+1/2}. \end{cases} \end{aligned} \tag{4}$$

This generalisation of the Riemann problem is twofold: (i) the governing equations include non-linear advection as well as reaction terms and (ii) the initial condition consists of two reconstruction polynomials of $(r-1)$th order for a scheme of rth order of accuracy. By the order of accuracy we mean the convergence rate of the scheme when the mesh is refined with a *fixed* Courant number.

We find an approximate solution for the interface state $q(x_{i+1/2},\tau)$, where τ is local time $\tau = t - t^n$, using a semi-analytical method [26]. The method gives the solution at $x = x_{i+1/2}$ at a time τ, assumed to be sufficiently small, in terms of solutions of a sequence of *conventional* Riemann problems for *homogeneous* advection equations. First, we write a Taylor expansion of the interface state in time:

$$q(x_{i+1/2},\tau) = q(x_{i+1/2},0+) + \sum_{k=1}^{r-1}\left[\partial_t^{(k)} q(x_{i+1/2},0+)\right]\frac{\tau^k}{k!}, \quad \partial_t^{(k)} q(x,t) = \frac{\partial^k}{\partial t^k} q(x,t), \tag{5}$$

where $0+ \equiv \lim_{t\to 0+} t$. The leading term $q(x_{i+1/2}, 0+)$ accounts for the interaction of the boundary extrapolated values $q_{\mathrm{L}}(x_{i+1/2})$ and $q_{\mathrm{R}}(x_{i+1/2})$ and is the self-similar solution of the *conventional* Riemann problem with the piecewise constant data:

$$\begin{aligned} &\partial_t q + \partial_x f(q) = 0, \\ &q(x,0) = \begin{cases} q_{\mathrm{L}}(x_{i+1/2}) & \text{if } x < x_{i+1/2}, \\ q_{\mathrm{R}}(x_{i+1/2}) & \text{if } x > x_{i+1/2}, \end{cases} \end{aligned} \tag{6}$$

evaluated at $(x-x_{i+1/2})/t = 0$. We call $q(x_{i+1/2}, 0+)$ the Godunov state [5]. Next, to compute the remaining terms, we replace all time derivatives by spatial derivatives using Eq. (1) by means of the Cauchy–Kowalewski procedure. This procedure can be easily carried out with the aid of algebraic manipulators, such as MAPLE or Mathematica. For example, for the model inviscid reactive Burgers' equation

$$q_t + \left(\frac{1}{2}q^2\right)_x = Aq, \quad A = \text{constant}, \tag{7}$$

the Cauchy–Kowalewski procedure yields the following expressions for time derivatives:

$$\begin{aligned} q_t &= -qq_x + Aq, \\ q_{tt} &= 2qq_x^2 - 3q_xAq + q^2q_{xx} + A^2q \end{aligned} \tag{8}$$

and so on. Expressions (8) contain unknown (sought) spatial derivatives of the solution

$$q^{(k)} \equiv \frac{\partial^k}{\partial x^k} q, \quad q^{(1)} \equiv q_x, \quad q^{(2)} \equiv q_{xx}, \quad q^{(3)} \equiv q_{xxx}, \ldots$$

at cell interface position $x_{i+1/2}$ and time $\tau = 0$. It can be shown that by differentiating the governing equation with respect to x we can obtain evolution equations for each $q^{(k)}$. Generally, these evolution equations are non-linear and inhomogeneous: for a fixed $k > 0$ the source terms depend on lower-order derivatives $q^{(k-1)}$ and $q^{(k-2)}$, etc. For each k we then pose a generalized Riemann problem with initial conditions obtained by taking appropriate derivatives of $q_{\mathrm{L}}(x), q_{\mathrm{R}}(x)$ with respect to x; we call these problems *derivative* Riemann problems [25]. Because we only need the Godunov state of these derivative Riemann problems we can replace them by the following *linear*, homogeneous conventional Riemann problem:

$$\begin{aligned} &\partial_t q^{(k)} + \lambda_{i+1/2}\partial_x q^{(k)} = 0, \quad \lambda_{i+1/2} = \frac{\partial f(q)}{\partial q}(q(x_{i+1/2}, 0+)), \\ &q^{(k)}(x,0) = \begin{cases} \partial_x^{(k)} q_{\mathrm{L}}(x_{i+1/2}), & x < x_{i+1/2}, \\ \partial_x^{(k)} q_{\mathrm{R}}(x_{i+1/2}), & x > x_{i+1/2}, \end{cases} \\ &k = 1, \ldots, r-1. \end{aligned} \tag{9}$$

Having found the solution at $x = x_{i+1/2}$ of all these derivative Riemann problems we substitute them into Taylor expansion (5) and obtain an approximate solution $q_{i+1/2}(\tau)$:

$$q_{i+1/2}(\tau) = a_0 + a_1\tau + a_2\tau^2 + \cdots + a_{r-1}\tau^{r-1}, \quad 0 \leqslant \tau \leqslant \Delta t, \ \ a_i = \text{constant}, \tag{10}$$

which approximates the interface state $q(x_{i+1/2}, \tau)$ to the rth order of accuracy

$$q_{i+1/2}(\tau) = q(x_{i+1/2}, \tau) + \mathrm{O}(\tau^r), \quad 0 \leqslant \tau \leqslant \Delta t. \tag{11}$$

Two options exist to evaluate the numerical flux. The first option is the *state-expansion* ADER [19], in which an appropriate rth-order accurate Gaussian rule is used to evaluate the numerical flux

$$\hat{f}_{i+1/2} = \sum_{\alpha=0}^{N} f(q_{i+1/2}(\gamma_\alpha \Delta t)) K_\alpha, \tag{12}$$

where γ_j and K_α are properly scaled nodes and weights of the rule and N is the number of nodes.

The second option to evaluate the numerical flux is the *flux-expansion* ADER [27,18], in which we seek Taylor time expansion of the physical flux at $x_{i+1/2}$:

$$f(x_{i+1/2}, \tau) = f(x_{i+1/2}, 0+) + \sum_{k=1}^{r-1} \left[\partial_t^{(k)} f(x_{i+1/2}, 0+)\right] \frac{\tau^k}{k!}. \tag{13}$$

From (13) and the second equation in (3) the numerical flux is now given by

$$f_{i+1/2} = f(x_{i+1/2}, 0+) + \sum_{k=1}^{r-1} \left[\partial_t^{(k)} f(x_{i+1/2}, 0+)\right] \frac{\Delta t^k}{(k+1)!}. \tag{14}$$

The leading term $f(x_{i+1/2}, 0+)$ accounts for the first-instant interaction of left and right boundary extrapolated values and is computed from (6) using a monotone flux, such as Godunov's first-order upwind flux. Following [27], the remaining higher-order time derivatives of the flux in (14) are expressed via time derivatives of the intercell state $q_{i+1/2}(\tau)$:

$$\frac{\partial}{\partial t} f = \frac{\partial f}{\partial q} \frac{\partial}{\partial t} q, \quad \frac{\partial^2}{\partial t^2} f = \frac{\partial^2 f}{\partial q^2} \left(\frac{\partial}{\partial t} q\right)^2 + \frac{\partial f}{\partial q} \frac{\partial^2}{\partial t^2} q, \tag{15}$$

where from (10)

$$\frac{\partial}{\partial t} q = a_1, \quad \frac{\partial^2}{\partial t^2} q = a_2, \tag{16}$$

and so on. No numerical quadrature is then required to compute the numerical flux.

An improvement of the flux-expansion ADER approach is the so-called ADER-TVD approach [27]. In ADER-TVD schemes all terms in the flux expansion (14) are computed not as a first-order upwind flux, but as a second-order TVD flux with a compressive limiter, such as the flux of the weighted average flux scheme [22,23].

Now we deal with the treatment of the source term. The first step in the evaluation of the numerical source term s_i^n in (3) is to discretize the space integral by means of a N-point Gaussian rule [20]

$$s_i = \sum_{\alpha=1}^{N} \left(\frac{1}{\Delta t} \int_{t^n}^{t^{n+1}} s(x_\alpha, \tau, q(x_\alpha, \tau)) \mathrm{d}\tau \right) K_\alpha, \tag{17}$$

where K_α are the scaled weights of the rule, x_α are the Gaussian integration points and N is the total number of points in the rule.

Next for each Gaussian point x_α (which are different from $x_{i\pm1/2}$) we reconstruct values of q and its spatial derivatives by means of the WENO reconstruction, write the time Taylor expansion of the form (5) and perform the Cauchy–Kowalewski procedure to replace all time derivatives by spatial derivatives. As a result we obtain high-order approximations to $q(x_\alpha, \tau)$, $\alpha = 1, \ldots, N$ of the form (10). Finally, the time integration in (17) is carried out by means of a Gaussian quadrature

$$s_i = \sum_{\alpha=1}^{N} \left(\sum_{l=1}^{N} s(x_\alpha, \tau_l, q(x_\alpha, \tau_l)) K_l \right) K_\alpha. \tag{18}$$

The solution is advanced by one time step by updating the cell averages of the solution according to the one-step formula (2).

Remark: We note that for *one-dimensional homogeneous* non-linear systems the ADER approach has some similarities with finite volume ENO schemes of Harten et al. [8] in that both methods use the Cauchy–Kowalewski procedure to convert spatial derivatives into temporal derivatives. The key difference between methods lies in how time accuracy is preserved. We refer the reader to [19] for a more detailed comparison.

3. Three-space dimensions

Consider the following three-dimensional nonlinear advection–reaction equation:

$$\partial_t q + \partial_x f(q) + \partial_y g(q) + \partial_z h(q) = s(x, y, z, t, q). \tag{19}$$

Integration of (19) over the control volume $I_{ijk} \times \Delta t$, with

$$I_{ijk} = [x_{i-1/2}, x_{i+1/2}] \times [y_{j-1/2}, y_{j+1/2}] \times [z_{k-1/2}, z_{k+1/2}],$$

of dimensions

$$\Delta x = x_{i+1/2} - x_{i-1/2}, \quad \Delta y = y_{j+1/2} - y_{j-1/2}, \quad \Delta z = z_{k+1/2} - z_{k-1/2}, \quad \Delta t = t^{n+1} - t^n,$$

gives

$$q_{ijk}^{n+1} = q_{ijk}^n + \frac{\Delta t}{\Delta x}(f_{i-1/2,jk} - f_{i+1/2,jk}) + \frac{\Delta t}{\Delta y}(g_{i,j-1/2,k} - g_{i,j+1/2,k}) + \frac{\Delta t}{\Delta z}(h_{ij,k-1/2} - h_{ij,k+1/2}) + \Delta t\, s_{ijk}, \tag{20}$$

where q_{ijk}^n, $f_{i+1/2,jk}$, $g_{i,j+1/2,k}$, $h_{ij,k+1/2}$ and s_{ijk} are given by

$$q_{ijk}^n = \frac{1}{\Delta x}\frac{1}{\Delta y}\frac{1}{\Delta z}\int_{x_{i-1/2}}^{x_{i+1/2}}\int_{y_{j-1/2}}^{y_{j+1/2}}\int_{y_{j-1/2}}^{y_{j+1/2}} q(x, y, z, t^n)\mathrm{d}z\,\mathrm{d}y\,\mathrm{d}x, \tag{21}$$

$$\begin{aligned}
f_{i+1/2,j,k} &= \frac{1}{\Delta t}\frac{1}{\Delta y}\frac{1}{\Delta z}\int_{y_{j-1/2}}^{y_{j+1/2}}\int_{z_{k-1/2}}^{z_{k+1/2}}\int_{t^n}^{t^{n+1}} f(q(x_{i+1/2}, y, z, \tau))\mathrm{d}\tau\,\mathrm{d}z\,\mathrm{d}y,\\
g_{i,j+1/2,k} &= \frac{1}{\Delta t}\frac{1}{\Delta x}\frac{1}{\Delta z}\int_{x_{i-1/2}}^{x_{i+1/2}}\int_{z_{k-1/2}}^{z_{k+1/2}}\int_{t^n}^{t^{n+1}} g(q(x, y_{i+1/2}, z, \tau))\mathrm{d}\tau\,\mathrm{d}z\,\mathrm{d}x,\\
h_{ij,k+1/2} &= \frac{1}{\Delta t}\frac{1}{\Delta x}\frac{1}{\Delta y}\int_{x_{i-1/2}}^{x_{i+1/2}}\int_{y_{j-1/2}}^{y_{j+1/2}}\int_{t^n}^{t^{n+1}} h(q(x, y, z_{i+1/2}, \tau))\mathrm{d}\tau\,\mathrm{d}y\,\mathrm{d}x,
\end{aligned} \tag{22}$$

$$s_{ijk} = \frac{1}{\Delta t}\frac{1}{\Delta x}\frac{1}{\Delta y}\frac{1}{\Delta z}\int_{t^n}^{t^{n+1}}\int_{x_{i-1/2}}^{x_{i+1/2}}\int_{y_{j-1/2}}^{y_{j+1/2}}\int_{z_{k-1/2}}^{z_{k+1/2}} s(x, y, z, t, q)\mathrm{d}z\,\mathrm{d}y\,\mathrm{d}x\,\mathrm{d}t. \tag{23}$$

The procedure to evaluate the numerical flux in three-space dimensions consists of three main steps. We concentrate on $f_{i+1/2,jk}$; the expressions for $g_{i,j+1/2,k}$, $h_{ij,k+1/2}$ are obtained in an entirely analogous manner. First we discretize the spatial integrals over the cell faces in (22) using a tensor product of a suitable Gaussian numerical quadrature. The expression for the numerical flux in the x coordinate direction then reads

$$f_{i+1/2,jk} = \sum_{\alpha=1}^{N}\sum_{\beta=1}^{N}\left(\frac{1}{\Delta t}\int_{t^n}^{t^{n+1}} f(q(x_{i+1/2}, y_\alpha, z_\beta, \tau))\mathrm{d}\tau\right)K_\beta K_\alpha, \tag{24}$$

where y_α, z_β are the integration points over the cell face $[x_{i-1/2}, x_{i+1/2}] \times [y_{j-1/2}, y_{j+1/2}]$ and K_α, K_β are the weights. Next we reconstruct the pointwise values of the solution from cell averages to high order of

accuracy at the Gaussian integration points $(x_{i+1/2}, y_\alpha, z_\beta)$, including all derivatives up to order $r-1$ for the scheme of rth order of accuracy. In this paper we use the so-called dimension-by-dimension reconstruction which is explained in [2,16] in the context of the two-dimensional ENO and WENO schemes. Reconstruction in three-space dimensions is a straightforward generalization of the two-dimensional algorithm and consists of three one-dimensional sweeps [21]. First we perform a one-dimensional WENO sweep in the x direction (normal to the face) and obtain left and right y–z averages of q and its x derivatives. Then we perform the one-dimensional sweep in y direction to obtain z averages of q and its mixed x–y derivatives for Gaussian integration points in y direction. Finally, we obtain the sought pointwise values by performing the one-dimensional WENO sweep in z direction. See [21] for more details.

After the reconstruction is carried out for each Gaussian integration point (y_α, z_β) at the cell face we pose the generalized Riemann problem (4) in the x-coordinate direction (normal to the cell boundary) and obtain a high-order approximation to $q(x_{i+1/2}, y_\alpha, z_\beta, \tau)$. All steps of the solution procedure remain *essentially* as in the one-dimensional case. First, we write a Taylor series expansion in time for the solution

$$q(x_{i+1/2}, y_\alpha, z_\beta, \tau) = q(x_{i+1/2}, y_\alpha, z_\beta, 0+) + \sum_{k=1}^{r-1} [\partial_t^{(k)} q(x_{i+1/2}, y_\alpha, z_\beta, 0+)] \frac{\tau^k}{k!}. \tag{25}$$

The leading term $q(x_{i+1/2}, y_\alpha, z_\beta, 0+)$ is the self-similar solution of the conventional Riemann problem

$$\begin{aligned} &\partial_t q + \partial_x f(q) = 0, \\ &q(x,0) = \begin{cases} q_{\mathrm{L}}(x_{i+1/2}, y_\alpha, z_\beta) & \text{if } x < x_{i+1/2}, \\ q_{\mathrm{R}}(x_{i+1/2}, y_\alpha, z_\beta) & \text{if } x > x_{i+1/2}, \end{cases} \end{aligned} \tag{26}$$

evaluated at $(x - x_{i+1/2})/t = 0$. Next, we replace all time derivatives by space derivatives using (19) by means of the Cauchy–Kowalewski procedure which will now involve mixed x, y and z derivatives up to order $r-1$. For example, for the inviscid reactive Burgers' equation

$$q_t + \left(\frac{1}{2}q^2\right)_x + \left(\frac{1}{2}q^2\right)_y + \left(\frac{1}{2}q^2\right)_z = Aq, \tag{27}$$

the Cauchy–Kowalewski procedure yields the following expressions for time derivatives:

$$\begin{aligned} q_t &= -qq_x - qq_y - qq_z + Aq, \\ q_{tt} &= q_x q q_z + 2qq_x^2 + q^2 q_{xx} + 2q^2 q_{xy} + 2q^2 q_x z + 2qq_y^2 + q^2 q_{yy} + 2q^2 q_y z \\ &\quad + 2qq_z^2 + q^2 q_{zz} + A^2 q - 3q_x Aq + 4q_y qq_z - 3q_z Aq + 4q_x qq_y - 3q_y Aq, \end{aligned} \tag{28}$$

and so on. The expressions in (28) contain space derivatives of the solution

$$q^{(k_1,k_2,k_3)} = \frac{\partial^{k_1+k_2+k_3}}{\partial x^{k_1} \partial y^{k_2} \partial z^{k_3}} q, \quad q^{(1,0,0)} \equiv q_x, \quad q^{(0,1,0)} \equiv q_y, \quad q^{(0,0,1)} \equiv q_z, \ldots \tag{29}$$

It can be shown that all $q^{(k_1,k_2,k_3)}$ obey inhomogeneous evolution equations, which are obtained by taking spatial derivatives of the governing equation. Then all $q^{(k_1,k_2,k_3)}$ can be computed as the Godunov states of the following linear, derivative Riemann problems:

$$\begin{aligned} &\partial_t q^{(k_1,k_2,k_3)} + \lambda_{i+1/2,\alpha\beta} \partial_x q^{(k_1,k_2,k_3)} = 0, \quad \lambda_{i+1/2,\alpha\beta} = \frac{\partial f(q)}{\partial q}(q(x_{i+1/2}, y_\alpha, z_\beta, 0+)), \\ &q^{(k_1,k_1,k_3)}(x,0) = \begin{cases} \frac{\partial^{k_1+k_2+k_3}}{\partial x^{k_1} \partial y^{k_2} \partial z^{k_3}} q_{\mathrm{L}}(x_{i+1/2}, y_\alpha, z_\beta), & x < x_{i+1/2}, \\ \frac{\partial^{k_1+k_2+k_3}}{\partial x^{k_1} \partial y^{k_2} \partial z^{k_3}} q_{\mathrm{R}}(x_{i+1/2}, y_\alpha, z_\beta), & x > x_{i+1/2}. \end{cases} \end{aligned} \tag{30}$$

Here, the initial conditions

$$\frac{\partial^{k_1+k_2+k_3}}{\partial x^{k_1}\partial y^{k_2}\partial z^{z_3}} q_{\mathrm{L}}(x_{i+1/2}, y_\alpha, z_\beta), \quad \frac{\partial^{k_1+k_2+k_3}}{\partial x^{k_1}\partial y^{k_2}\partial z^{z_3}} q_{\mathrm{R}}(x_{i+1/2}, y_\alpha, z_\beta)$$

are left and right reconstructed pointwise values of derivatives. After solving (30) for $1 \leqslant k_1 + k_2 + k_3 \leqslant r - 1$ we substitute $q^{(k_1,k_2,k_3)}$ into the Taylor expansion (25) and form a polynomial $q_{i+1/2,\alpha,\beta}(\tau)$:

$$q_{i+1/2,\alpha,\beta}(\tau) = c_0 + c_1\tau + c_2\tau^2 + \cdots + c_{r-1}\tau^{r-1}, \quad 0 \leqslant \tau \leqslant \Delta t, \;\; c_i = \text{constant}, \tag{31}$$

which approximates the interface state $q(x_{i+1/2}, y_\alpha, z_\beta, \tau)$ at the Gaussian integration point $(x_{i+1/2}, y_\alpha, z_\beta)$ to rth order of accuracy.

The flux of the *state-expansion* ADER scheme is given by

$$f_{i+1/2,jk} = \sum_{\alpha=1}^{N}\sum_{\beta=1}^{N}\left(\sum_{l=1}^{N} f(q(x_{i+1/2}, y_\alpha, z_\beta, \tau_l))K_l\right)K_\beta K_\alpha. \tag{32}$$

For the *flux expansion* ADER schemes we write Taylor time expansion of the physical flux at each point $(x_{i+1/2}, y_\alpha, z_\beta)$:

$$f(x_{i+1/2}, y_\alpha, z_\beta, \tau) = f(x_{i+1/2}, y_\alpha, z_\beta, 0+) + \sum_{k=1}^{r-1}\left[\partial_t^{(k)} f(x_{i+1/2}, y_\alpha, z_\beta, 0+)\right]\frac{\tau^k}{k!}. \tag{33}$$

Similar to the one-dimensional case, the leading term $f(x_{i+1/2}, y_\alpha, z_\beta, 0+)$ is computed from (26) using a monotone flux, such as Godunov's first-order upwind flux. The remaining higher-order time derivatives of the flux in (33) are expressed via time derivatives of the intercell state $q_{i+1/2,\alpha,\beta}(\tau)$. These time derivatives are computed from Taylor expansion (31). The numerical flux is then given by

$$f_{i+1/2,jk} = \sum_{\alpha=1}^{N}\sum_{\beta=1}^{N}\left(f(x_{i+1/2}, y_\alpha, z_\beta, 0+) + \sum_{k=1}^{r-1}\left[\partial_t^{(k)} f(x_{i+1/2}, y_\alpha, z_\beta, 0+)\right]\frac{\Delta t^k}{(k+1)!}\right)K_\alpha K_\beta. \tag{34}$$

The computation of the numerical source now involves four-dimensional integration. First, we use the tensor-product of the N-point Gaussian rule to discretize the three-dimensional space integral in (23) so that the expression for s_{ijk} reads

$$s_{ijk} = \sum_{\alpha=1}^{N}\sum_{\beta=1}^{N}\sum_{\gamma=1}^{N}\left(\frac{1}{\Delta t}\int_{t^n}^{t^{n+1}} s(x_\alpha, y_\beta, z_\gamma, \tau, q(x_\alpha, y_\beta, z_\gamma, \tau))\mathrm{d}\tau\right)K_\gamma K_\beta K_\alpha. \tag{35}$$

Then we reconstruct values and all spatial derivatives, including mixed derivatives, of q at the Gaussian integration point in x–y–z space for the time level t^n. Note that these points are different from flux integration points over cell faces. The reconstruction procedure is entirely analogous to that for the flux evaluation. Next for each Gaussian point $(x_\alpha, y_\beta, z_\gamma)$ we perform the Cauchy–Kowalewski procedure and replace time derivatives by space derivatives. As a result we have high-order approximations to $q(x_\alpha, y_\beta, z_\gamma, \tau)$. Finally, we carry out numerical integration in time using the Gaussian quadrature

$$s_{ijk} = \sum_{\alpha=1}^{N}\sum_{\beta=1}^{N}\sum_{\gamma=1}^{N}\left(\sum_{l=1}^{N} s(x_\alpha, y_\beta, z_\gamma, \tau_l, q(x_\alpha, y_\beta, z_\gamma, \tau_l))K_l\right)K_\gamma K_\beta K_\alpha. \tag{36}$$

The solution is advanced by one time step by updating the cell averages of the solution according to the one-step formula (20).

The explicit scheme considered above requires the computation of a time step Δt to be used in the conservative updates (2) and (20), such that stability of the numerical method is ensured. One way of choosing Δt is

$$\Delta t = C_{cfl} \times \min_{ijk} \left(\frac{\Delta x}{|\lambda_{ijk}^{n,x}|}, \frac{\Delta y}{|\lambda_{ijk}^{n,y}|}, \frac{\Delta z}{|\lambda_{ijk}^{n,z}|} \right). \tag{37}$$

Here $\lambda_{ijk}^{n,d}$ is the speed of the fastest wave present at time level n travelling in the d direction, with $d = x, y, z$. C_{cfl} is the CFL number and is chosen according to the linear stability condition of the scheme.

In one-space dimension linear schemes applied to the linear homogeneous advection equation with constant coefficient have the optimal stability condition $C_{\mathrm{cfl}} \leqslant 1$ [25]. Numerical experiments indicate that the approach has the same stability condition for nonlinear scalar equations and systems as well [19].

The linear stability analysis of ADER schemes in two- and three-space dimensions is not available yet. Numerical experiments indicate that ADER schemes have a reduced stability condition which in fact coincides with the stability condition of the unsplit Godunov scheme [5] and ENO/WENO schemes [2,16]. In two-space dimensions the stability condition is $0 < C_{\mathrm{cfl}} \leqslant 1/2$ and in three-space dimensions the stability condition is $0 < C_{\mathrm{cfl}} \leqslant 1/3$.

When the source term is present, this should also be taken into account when choosing a stable time step.

4. Numerical results

In this section we present numerical results of the state-expansion ADER schemes of up to fifth order of accuracy as applied to scalar equations with source terms. The detailed evaluation of the flux-expansion ADER in several space dimensions is the subject of ongoing research. These examples illustrate that the ADER schemes can compute discontinuous solutions without oscillations and at the same time maintain the designed very high order of accuracy in *both time and space* in multiple space dimensions. In all examples for flux and source term integration we use the two-point fourth-order Gaussian rule for third and fourth-order ADER schemes and the four-point eighth-order Gaussian rule for the fifth-order ADER scheme.

For comparisons in two-space dimensions we also run the finite-volume scheme of Shi et al. [16] with dimension-by-dimension piecewise parabolic ($r = 3$) reconstruction. In the original reference [16] this scheme uses the upwind Rusanov flux [13] as the building block and a three-point (sixth-order) Gaussian quadrature to discretize fluxes and thus is of formal fifth order of accuracy in space. In this paper we use the exact Riemann solver in the framework of this scheme.

In all computations below we use a fixed Courant number $C_{\mathrm{cfl}} = 0.45$ in two-space dimensions and $C_{\mathrm{cfl}} = 0.27$ in three-space dimensions.

4.1. The two-dimensional inviscid Burgers' equation with a source term

We solve the two-dimensional inviscid Burgers' equation with a time-dependent source term

$$\begin{aligned} &q_t + \left(\frac{1}{2}q^2\right)_x + \left(\frac{1}{2}q^2\right)_y = S(x,y,t,q), \\ &S(x,y,t,q) = \pi(q-1)[\cos\pi(x-t)\sin\pi(y-t) + \sin\pi(x-t)\cos\pi(y-t)] \end{aligned} \tag{38}$$

with the following initial condition defined on $[-1,1]\times[-1,1]$:

$$q(x,y,0) = q_0(x,y) = \sin(\pi x)\sin(\pi y) \tag{39}$$

and periodic boundary conditions. The exact solution is $q(x,y,t) = q_0(x-t, y-t)$. The cell averages of the exact solution at the output time are computed by eighth-order Gaussian rule and are used to measure the numerical errors of the schemes.

Table 1 shows the errors at the output time $t = 1$. We observe that all ADER schemes reach the design rth order of accuracy in both L_∞ and L_1 norms. Moreover, the error decreases by an order of magnitude when the formal order of accuracy increases. As expected, the fifth-order ADER scheme is the most accurate scheme.

The solution of this problem varies rapidly with time and thus preserving the time accuracy of the numerical schemes is essential for obtaining the desired order of accuracy.

4.2. The three-dimensional inviscid Burgers' equation

We solve the three-dimensional inviscid Burgers' equation

$$q_t + \left(\frac{1}{2}q^2\right)_x + \left(\frac{1}{2}q^2\right)_y + \left(\frac{1}{2}q^2\right)_z = 0 \tag{40}$$

with the following initial condition defined on $[-1,1]\times[-1,1]\times[-1,1]$:

$$q(x,y,z,0) = q_0(x,y,z) = 0.25 + \sin(\pi x)\sin(\pi y)\sin(\pi z) \tag{41}$$

and periodic boundary conditions. For this test problem the exact solution is obtained by solving numerically the relation $q = q_0(x-qt, y-qt, z-qt)$ for a given point (x,y,z) and time t. The cell averages of the exact solution at the output time are computed using the eighth-order Gaussian rule.

Table 2 shows the errors at the output time $t = 0.05$, when the solution is still smooth. We observe that all ADER schemes reach the design rth order of accuracy in both norms. Moreover, the error decreases by an order of magnitude when the formal order of accuracy increases. As expected, the fifth-order scheme is the most accurate scheme.

Table 1
Convergence study for the 2D inviscid Burgers' equation with a source term (38) with initial condition (39) at output time $t = 1$. CFL = 0.45 for all schemes

Method	N	L_∞ error	L_∞ order	L_1 error	L_1 order
ADER3	10	1.90×10^{-2}		3.21×10^{-2}	
	20	2.60×10^{-3}	2.87	3.99×10^{-3}	3.01
	40	3.43×10^{-4}	2.92	4.78×10^{-4}	3.06
	80	4.15×10^{-5}	3.05	5.90×10^{-5}	3.02
	160	5.11×10^{-6}	3.02	7.36×10^{-6}	3.00
ADER4	10	7.00×10^{-3}		3.51×10^{-3}	
	20	1.82×10^{-4}	5.26	6.62×10^{-5}	5.73
	40	5.53×10^{-6}	5.04	2.00×10^{-6}	5.05
	80	1.62×10^{-7}	5.10	9.40×10^{-8}	4.41
	160	7.59×10^{-9}	4.41	5.60×10^{-9}	4.07
ADER5	10	5.46×10^{-4}		4.66×10^{-4}	
	20	2.41×10^{-5}	4.50	2.69×10^{-5}	4.11
	40	8.86×10^{-7}	4.77	8.96×10^{-7}	4.91
	80	2.88×10^{-8}	4.95	2.81×10^{-8}	5.00
	160	9.08×10^{-10}	4.99	8.77×10^{-10}	5.00

N is the number of cells in each coordinate direction.

Table 2
Convergence study for the 3D inviscid Burgers' equation (40) with initial condition (41) at output time $t = 0.05$. CFL = 0.27 for all schemes

Method	N	L_∞ error	L_∞ order	L_1 error	L_1 order
ADER3	5	1.84×10^{-2}		3.34×10^{-2}	
	10	2.05×10^{-3}	3.17	3.47×10^{-3}	3.27
	20	3.89×10^{-4}	2.39	2.09×10^{-4}	4.05
	40	4.85×10^{-5}	3.00	1.74×10^{-5}	3.59
	80	6.99×10^{-6}	2.79	2.18×10^{-6}	3.00
ADER4	5	1.90×10^{-2}		2.21×10^{-2}	
	10	1.07×10^{-3}	4.14	5.82×10^{-4}	5.25
	20	6.64×10^{-5}	4.01	2.25×10^{-5}	4.70
	40	5.10×10^{-6}	3.70	1.27×10^{-6}	4.15
	80	3.07×10^{-7}	4.05	8.27×10^{-8}	3.94
ADER5	5	4.77×10^{-3}		7.96×10^{-3}	
	10	2.42×10^{-4}	4.30	1.17×10^{-4}	6.09
	20	1.07×10^{-5}	4.50	3.50×10^{-6}	5.06
	40	2.75×10^{-7}	5.28	1.06×10^{-7}	5.04
	80	8.79×10^{-9}	4.97	3.95×10^{-9}	4.75

N is the number of cells in each coordinate direction.

4.3. The kinematic frontogenesis problem

This problem [6] is a popular test in meteorology, where it models a real effect taking place in the Earth atmosphere. From the numerical point of view it tests the ability of the schemes to handle sharp moving fronts in two-space dimensions.

We solve the two-dimensional linear equation with variable coefficients

$$q_t + (u(x,y)q)_x + (v(x,y)q)_y = 0, \tag{42}$$

where (u,v) is a steady divergence-free velocity field:

$$\begin{aligned} &u = -y\omega(r), \quad v = x\omega(r), \quad \omega(r) = \frac{1}{r}U_T(r), \quad r^2 = x^2 + y^2, \\ &U_T(r) = U_{\max}\,\mathrm{sech}^2(r)\tanh(r), \quad U_{\max} = 2.5980762. \end{aligned} \tag{43}$$

The initial distribution of $q(x,y,t)$, defined on a square domain $[-5,5]\times[-5,5]$, is assumed to be one-dimensional

$$q(x,y,0) = q_0(y) = \tanh\left(\frac{y}{\delta}\right), \tag{44}$$

where δ expresses the characteristic width of the front zone. The exact solution is then given by [6]

$$q(x,y,t) = q_0(y\cos(\omega t) - x\sin(\omega t)), \tag{45}$$

and represents the rotation of the initial distribution around the origin with variable angular velocity $\omega(r)$. We note that as time evolves the solution will eventually develop scales which will be beyond the resolution of the computational mesh.

We first consider a smooth solution with $\delta = 1$. Table 3 shows a convergence study for cell averages at the output time $t = 4$. Obviously, all ADER schemes achieve the designed order of accuracy. The size of the error decreases as the formal order of the scheme increases. Moreover, the fourth- and fifth-order schemes show sixth order of accuracy on fine meshes. We see that the third-order ADER3 scheme competes well

Table 3
Convergence study for the 2D linear advection equation with variable coefficients (42) with initial condition (44) and $\delta = 1$ at output time $t = 4$. CFL = 0.45 for all schemes

Method	N	L_∞ error	L_∞ order	L_1 error	L_1 order
ADER3	50	2.92×10^{-1}		6.53×10^{-1}	
	100	7.56×10^{-2}	1.95	1.16×10^{-1}	2.49
	200	9.27×10^{-3}	3.03	1.12×10^{-2}	3.38
	400	7.47×10^{-4}	3.63	6.65×10^{-4}	4.07
ADER4	50	2.04×10^{-1}		3.67×10^{-1}	
	100	2.95×10^{-2}	2.79	3.95×10^{-2}	3.22
	200	2.63×10^{-3}	3.49	2.51×10^{-3}	3.98
	400	3.22×10^{-5}	6.35	2.57×10^{-5}	6.61
ADER5	50	1.36×10^{-1}		2.84×10^{-1}	
	100	2.10×10^{-2}	2.69	3.06×10^{-2}	3.21
	200	1.26×10^{-3}	4.06	9.47×10^{-4}	5.01
	400	2.08×10^{-5}	5.92	1.70×10^{-5}	5.80
WENO [16], exact Riemann solver	50	2.87×10^{-1}		6.80×10^{-1}	
	100	7.78×10^{-2}	1.88	1.23×10^{-1}	2.47
	200	9.82×10^{-3}	2.99	1.44×10^{-2}	3.10
	400	1.02×10^{-3}	3.27	1.86×10^{-3}	2.95

N is the number of cells in each coordinate direction.

with the WENO scheme and higher-order ADER schemes are considerably more accurate than the WENO scheme due to their higher-order spatial and temporal accuracy.

Next we compute the numerical solution which corresponds to a discontinuous initial distribution, with $\delta = 10^{-6}$. At the given output time the initial discontinuity has been rotated several times and the solution represents a discontinuous rolling surface.

Figs. 1 and 2 depict, respectively, a three-dimensional plot and contour plot of the numerical solution obtained by the fifth-order ADER scheme. We observe that the numerical solution is essentially non-oscillatory with sharp resolution of all discontinuities. All parts of the discontinuous rolling surface have been captured well. Further illustration is provided by Figs. 3–5, which show one-dimensional cuts along the y axis for $-3 \leqslant y \leqslant 3$; results of the third-, fourth- and fifth-order schemes on the meshes of 201×201 cells and 401×401 cells are shown. The odd number of cells is chosen so that the one-dimensional cut corresponds to the center of a middle cell for both meshes. In all figures the solid line corresponds to pointwise values of the exact solution, whereas symbols correspond to the numerical solution (cell averages). Clearly all schemes capture all features correctly. Note also that the resolution of the discontinuities improves as the formal order of accuracy of the scheme increases, which is more clearly shown in the finer mesh results. We observe slight oscillations in the result of the ADER5 scheme in the y cut of $q(x, y, t)$. These oscillations are due to the fact that the essentially non-oscillatory reconstruction cannot find a smooth stencil on this coarse mesh of 201×201 cells. Indeed, there are only four cells between discontinuities in the middle, whereas the fourth-order polynomials used in the reconstruction need at least five cells. When the mesh is refined further the oscillations vanish rapidly.

5. Extension to non-linear 2D systems

Finally, we would like to present some preliminary results on the possible extension of the ADER schemes of this paper to two-dimensional non-linear systems of the form

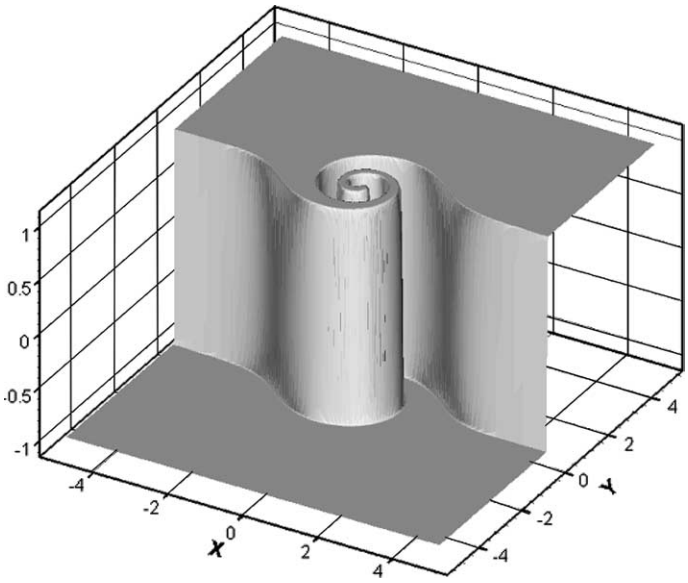

Fig. 1. Solution of the two-dimensional linear variable-coefficient advection equation (42) with the initial condition (44) and $\delta = 10^{-6}$ at output time $t = 4$ and CFL = 0.45. Method: the ADER5 scheme. Mesh of 401×401 cells is used.

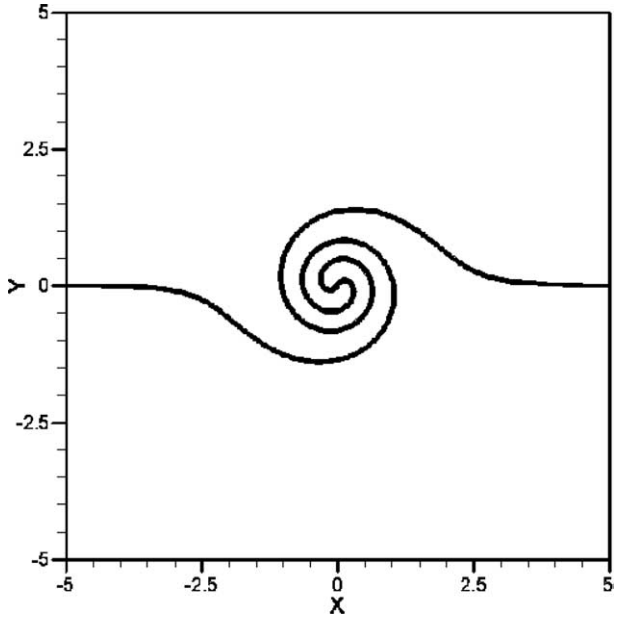

Fig. 2. Contours of the solution of the two-dimensional linear variable-coefficient advection equation (42) with the initial condition (44) and $\delta = 10^{-6}$ at output time $t = 4$ and CFL = 0.45. Method: the ADER5 scheme. Mesh of 401×401 cells is used. See also Fig. 1.

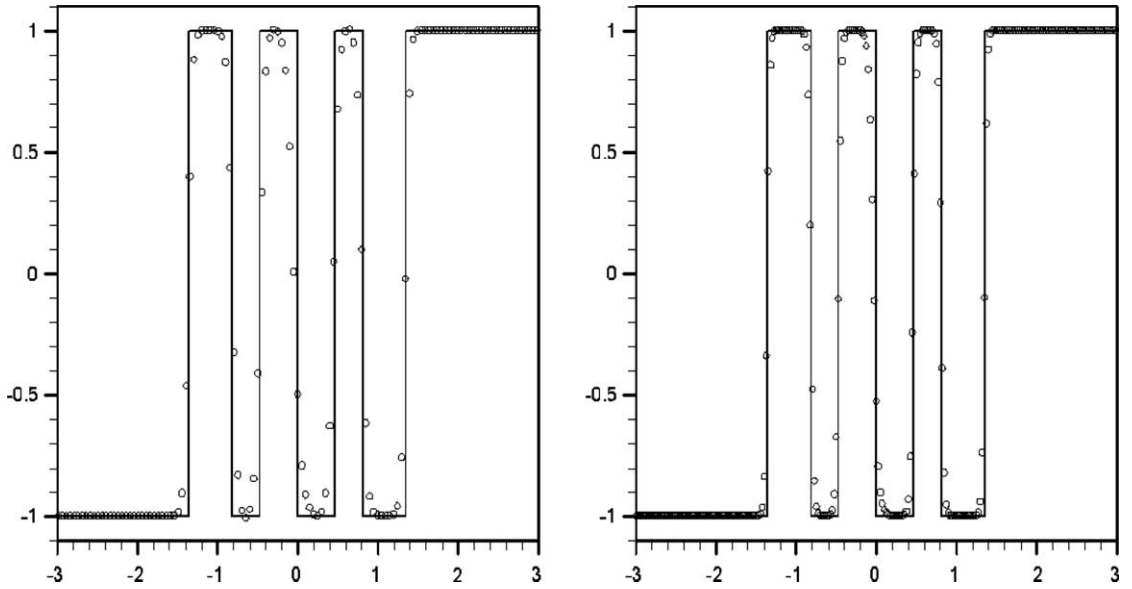

Fig. 3. One-dimensional cuts along the y axis for the two-dimensional linear variable-coefficient advection equation (42) with the initial condition (44) and $\delta = 10^{-6}$ at output time $t = 4$ and CFL = 0.45. Solid line shows pointwise values of the exact solution and symbols show cell averages computed by the ADER3 scheme. The meshes of 201×201 cells (left) and 401×401 cells (right) are used.

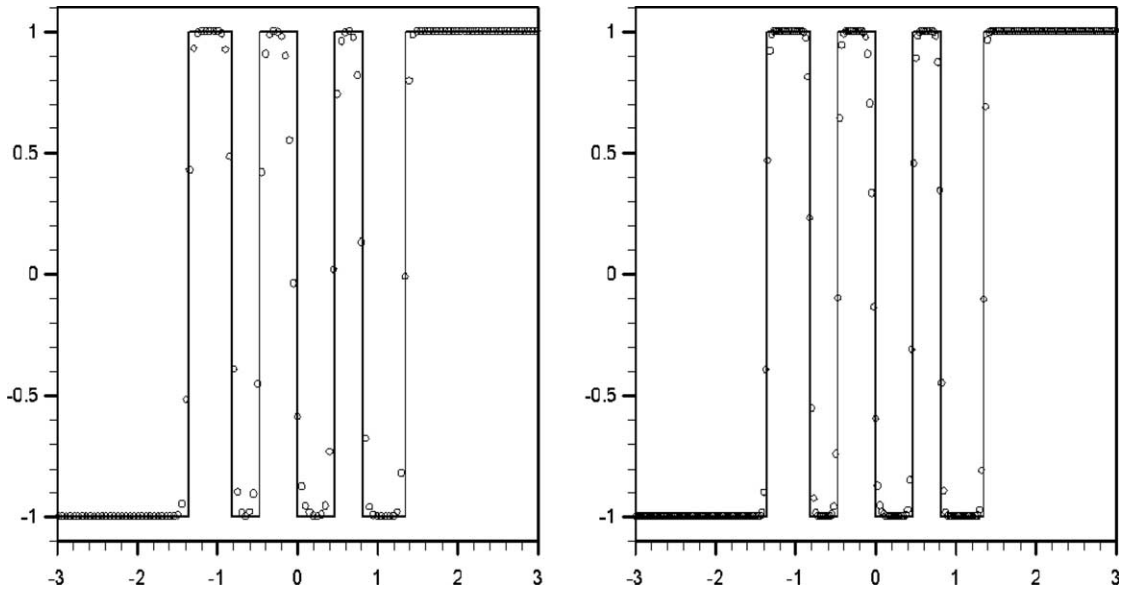

Fig. 4. One-dimensional cuts along the y axis for the two-dimensional linear variable-coefficient advection equation (42) with the initial condition (44) and $\delta = 10^{-6}$ at output time $t = 4$ and CFL = 0.45. Solid line shows pointwise values of the exact solution and symbols show cell averages computed by the ADER4 scheme. The meshes of 201×201 cells (left) and 401×401 cells (right) are used.

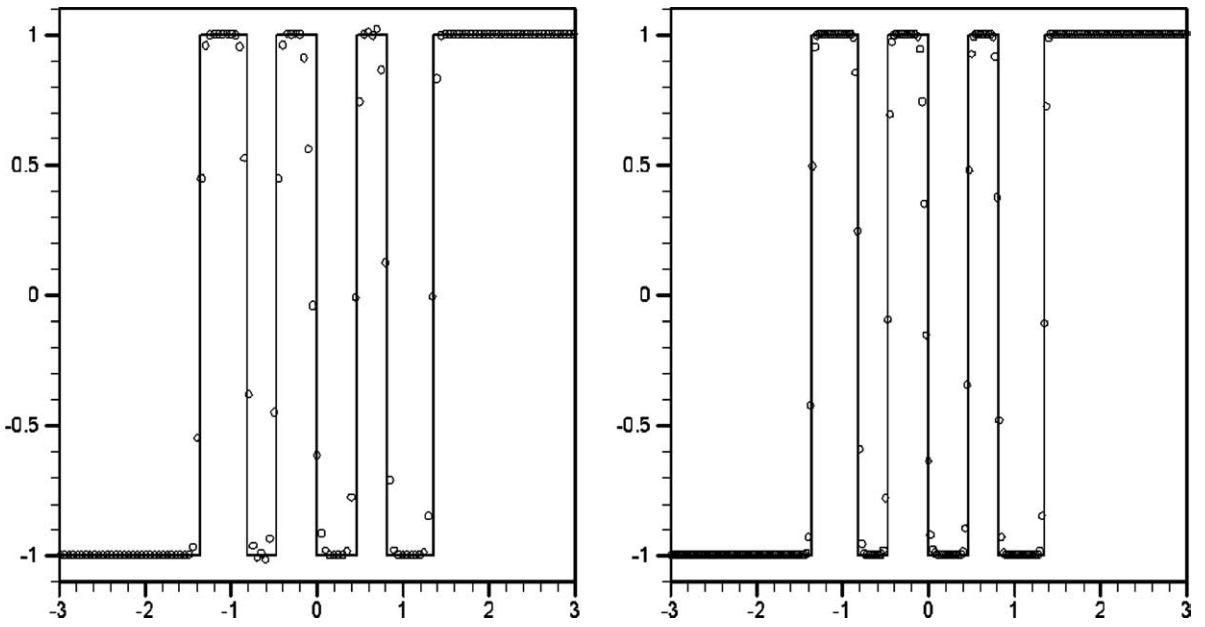

Fig. 5. One-dimensional cut along the y axis for the two-dimensional linear variable-coefficient advection equation (42) with the initial condition (44) and $\delta = 10^{-6}$ at output time $t = 4$ and CFL = 0.45. Solid line shows pointwise values of the exact solution and symbols show cell averages computed by the ADER5 scheme. The meshes of 201×201 cells (left) and 401×401 cells (right) are used.

$$\partial_t \mathbf{Q} + \partial_x \mathbf{F}(\mathbf{Q}) + \partial_y \mathbf{G}(\mathbf{Q}) = \mathbf{0}. \tag{46}$$

Similar to the two-dimensional scalar case, the scheme is written in the following one-step form:

$$\mathbf{Q}_{ij}^{n+1} = \mathbf{Q}_{ij}^{n} + \frac{\Delta t}{\Delta x}(\mathbf{F}_{i-1/2,j} - \mathbf{F}_{i+1/2,j}) + \frac{\Delta t}{\Delta y}(\mathbf{G}_{i,j-1/2} - \mathbf{G}_{i,j+1/2}), \tag{47}$$

where $\mathbf{Q}_{ij}^{n}$, $\mathbf{F}_{i+1/2,j}$ and $\mathbf{G}_{i,j+1/2}$ are given by

$$\mathbf{Q}_{ij}^{n} = \frac{1}{\Delta x}\frac{1}{\Delta y}\int_{x_{i-1/2}}^{x_{i+1/2}}\int_{y_{j-1/2}}^{y_{j+1/2}} \mathbf{Q}(x, y, t^n)\,\mathrm{d}y\,\mathrm{d}x, \tag{48}$$

$$\begin{aligned} \mathbf{F}_{i+1/2,j} &= \frac{1}{\Delta t}\frac{1}{\Delta y}\int_{y_{j-1/2}}^{y_{j+1/2}}\int_{t^n}^{t^{n+1}} \mathbf{F}(\mathbf{Q}(x_{i+1/2}, y, \tau))\,\mathrm{d}\tau\,\mathrm{d}y, \\ \mathbf{G}_{i,j+1/2} &= \frac{1}{\Delta t}\frac{1}{\Delta x}\int_{x_{i-1/2}}^{x_{i+1/2}}\int_{t^n}^{t^{n+1}} \mathbf{G}(\mathbf{Q}(x, y_{i+1/2}, \tau))\,\mathrm{d}\tau\,\mathrm{d}x. \end{aligned} \tag{49}$$

The evaluation of the ADER numerical flux $\mathbf{F}_{i+1/2,j}$ for non-linear systems is a straightforward extension of the scalar one and consists of the following steps. First we discretize the spatial integrals over the cell faces in (22) using a tensor product of a suitable Gaussian numerical quadrature. Next we reconstruct the pointwise values of the solution and all derivatives up to order $r-1$ from cell averages at the Gaussian integration points $(x_{i+1/2}, y_\alpha, z_\beta)$ by means of the dimension-by-dimension WENO reconstruction in characteristic variables. After the reconstruction is carried out for each Gaussian integration point (y_α, z_β) at the cell face we pose the generalised Riemann problem for the *augmented* non-linear system in the x-coordinate direction (normal to the cell boundary) and obtain a high-order approximation to $\mathbf{Q}(x_{i+1/2}, y_\alpha, z_\beta, \tau)$. All

steps of the solution procedure remain *essentially* as in the scalar two-dimensional case except that now we apply it to a non-linear system. The ADER flux is then evaluated by inserting the approximate state $\mathbf{Q}(x_{i+1/2}, y_\alpha, z_\beta, \tau)$ into the numerical quadrature.

As an example, we implement the third-order state-expansion ADER scheme as applied to the two-dimensional shallow-water equations, for which the vectors of conservative variables and fluxes are given by

$$\mathbf{Q} = \begin{pmatrix} h \\ hu \\ hv \end{pmatrix}, \quad \mathbf{F} = \begin{pmatrix} hu \\ hu^2 + \frac{1}{2}gh^2 \\ huv \end{pmatrix}, \quad \mathbf{G} = \begin{pmatrix} hv \\ hvu \\ hv^2 + \frac{1}{2}gh^2 \end{pmatrix}. \tag{50}$$

Here u and v are, respectively, x and y components of velocity, h is the depth and $g = 9.8$ is acceleration due to the gravity. For a review on the numerical methods for shallow water equations see [24].

We solve a circular dam-brake problem which corresponds to the following initial condition defined on $[-20{:}20] \times [-20{:}20]$:

$$h = \begin{cases} 2.5, & r \leqslant 2.5 \\ 0.5, & r > 2.5 \end{cases}, \quad u = v = 0, \quad r^2 = x^2 + y^2. \tag{51}$$

Here we compute the numerical solution at three output times $t = 0.4$, 1.4 and 4.7 on a mesh of 201 cells in each coordinate direction. We use $C_{\mathrm{cfl}} = 0.45$ for all runs. We compare the results of the ADER3 scheme with a reference radial solution, which is obtained by solving numerically the one-dimensional shallow-water equations with a geometric source term, on a very fine mesh. See Chapter 13 of [24] for details. Figs. 6–8 show a comparison between the one-dimensional reference radial solution (solid line) and the cell averages of the two-dimensional ADER3 solution (symbols) along the radial line that is coincident with the x-axis. We present distributions of depth h and velocity u. Additionally, Fig. 9 depicts the computed depth at the final output time $t = 4.7$.

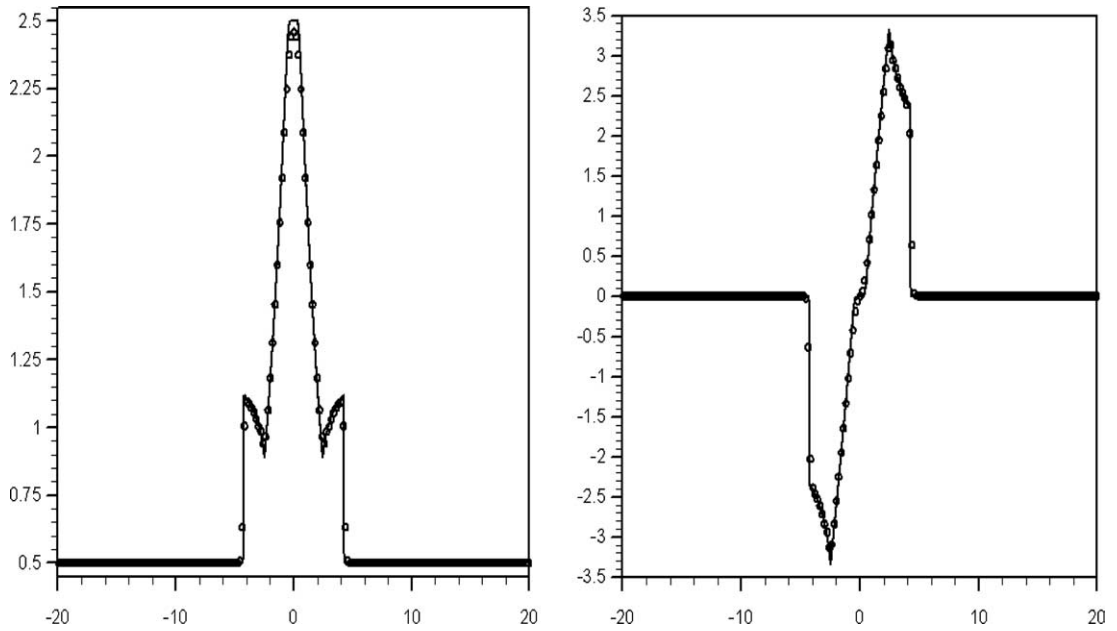

Fig. 6. The circular dam-break problem. Computed (symbol) and reference (line) solutions of depth (left) and velocity (right) for the ADER3 scheme at the output time $t = 0.4$.

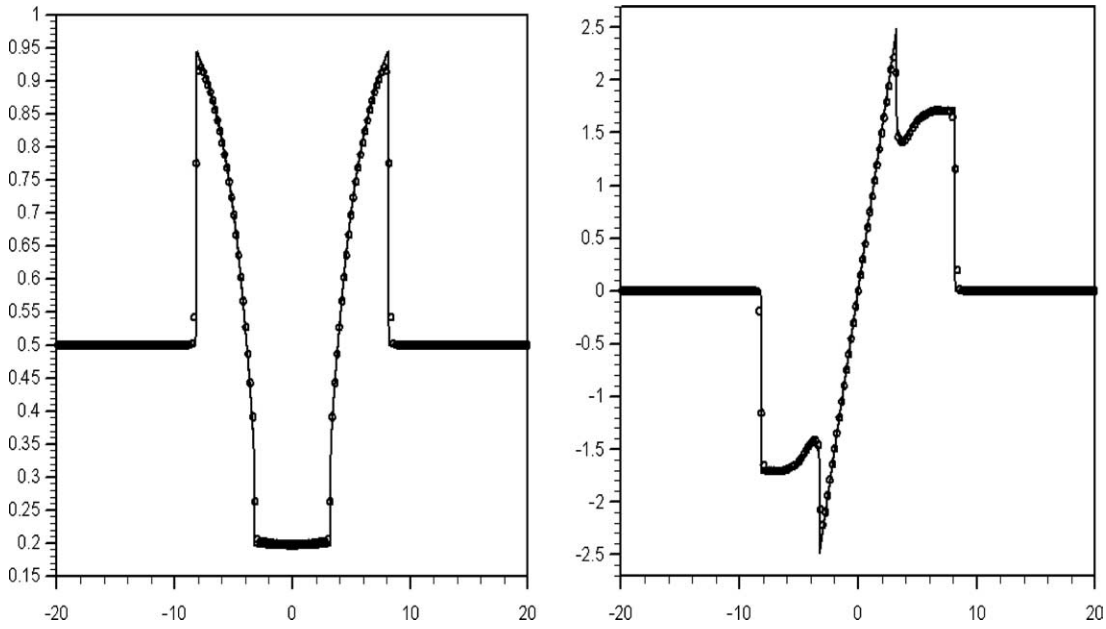

Fig. 7. The circular dam-break problem. Computed (symbol) and reference (line) solutions of depth (left) and velocity (right) for the ADER3 scheme at the output time $t = 1.4$.

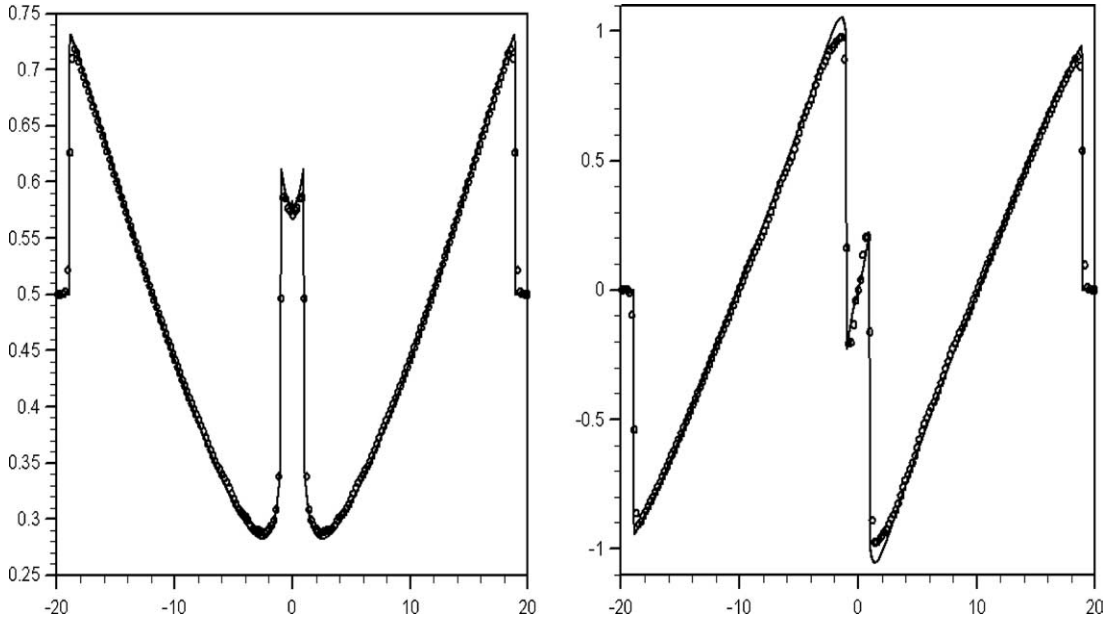

Fig. 8. The circular dam-break problem. Computed (symbol) and reference (line) solutions of depth (left) and velocity (right) for the ADER3 scheme at the output time $t = 4.7$.

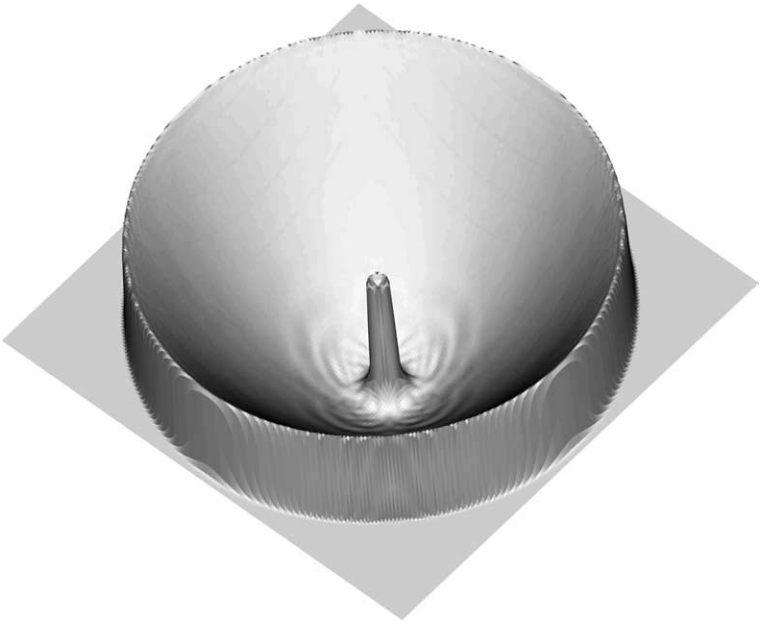

Fig. 9. The circular dam-break problem. Depth h at the output time $t = 4.7$.

A detailed numerical study of this problem for a sequence of output times is given in Chapter 13 of [24]. At time time $t = 0.4$, see Fig. 6, the solution contains an outward-propagating circular shock wave and an inward-propagation rarefaction wave which is about to reach the origin. By the time $t = 1.4$, see Fig. 7, the rarefaction has reflected from the origin and has overexpanded the flow to the point that the depth has fallen well below the ambient depth initially outside the circular dam. A secondary circular shock is then formed, which is more clearly seen in the velocity profile. This shock propagates inwards and at the final time $t = 4.7$ it has reflected from the centre and is propagating outwards.

We observe that the ADER3 scheme produces the correct flow pattern for all output times. A complex process of implosion of the circular shock in the center and formation of a reflected outward-moving circular shock does not lead to the generation of oscillations in the numerical solution. Overall representation of shocks is quite sharp, with only two to three cells across them.

Our numerical experiments show that in two-space dimensions the third-order ADER schemes are faster than the finite-volume WENO scheme roughly by a factor of 2. Additionally, ADER can typically take larger time steps in practical computations, usually by a factor of 2, which increases the difference in efficiency. Concerning the memory requirements we note that the ADER schemes of any order effectively need only two global arrays to store the vector of the conservative variables and the total sum of fluxes. This should be compared with the WENO schemes which need at least three arrays to store the data from stages of the TVD Runge–Kutta method. Also note that expensive memory transfer may be needed for the RK method to use only these three arrays.

Remark: It should be noted that in general finite-difference high-order schemes [7,1] are faster than the corresponding finite-volume schemes of the same spatial order of accuracy. For example, in two-space dimensions for spatially fifth-order WENO schemes the difference in efficiency is by a factor between three and four, depending on the computer and compiler used. However, the finite-difference schemes can only be applied on smooth structured meshes, whereas finite-volume schemes can be used on arbitrary unstructured non-uniform meshes. See e.g. [9,16] for finite-volume WENO schemes on triangular meshes.

6. Conclusions

The design of nonlinear ADER schemes of upto fifth order in both time and space as applied to scalar linear and nonlinear advection–reaction equations has been presented. The numerical results for the linear advection equation with variable coefficients and for the inviscid Burgers' equation with a time-dependent source term suggest that for smooth solutions the schemes retain the designed order of accuracy for realistic CFL numbers. When the solution is discontinuous the schemes produce essentially non-oscillatory results and sharp resolution of discontinuities. The extension to nonlinear hyperbolic systems in 2D and 3D is the subject of ongoing research. As shown here, preliminary results for two-dimensional shallow-water equations look promising.

Acknowledgements

Part of the paper was finalized during the stay of the second author at the Isaac Newton Institute for Mathematical Sciences, University of Cambridge and participation in the programme *Nonlinear Hyperbolic Waves in Phase Dynamics and Astrophysics*. The first author acknowledges the support provided by the Isaac Newton Institute for Mathematical Sciences, University of Cambridge, UK, as co-organizer of the six-month programme on *Nonlinear Hyperbolic Waves in Phase Dynamics and Astrophysics*, January to July 2003, and the associated EPSRC senior visiting fellowship, Grant No. GR N09276.

References

[1] D.S. Balsara, C.W. Shu, Monotonicity preserving weighted essentially non-oscillatory schemes with increasingly high order of accuracy, J. Comput. Phys 160 (2000) 405–452.
[2] J. Casper, H. Atkins, A finite-volume high order ENO scheme for two dimensional hyperbolic systems, J. Comput. Phys. 106 (1993) 62–76.
[3] B. Cockburn, C.-W. Shu, Runge–Kutta discontinuous Galerkin methods for convection-dominated problems, J. Sci. Comput. 16 (2001) 173–261.
[4] P. Colella, Multidimensional upwind methods for hyperbolic conservation laws, J. Comput. Phys. 87 (1990) 171–200.
[5] S.K. Godunov, A finite difference method for the computation of discontinuous solutions of the equations of fluid dynamics, Mat. Sbornik. 47 (1959) 357–393.
[6] R. Davies-Jones, Comments on 'A kinematic analysis of frontogenesis associated with a non-divergent vortex', J. Atm. Sci. 42 (1985) 2073–2075.
[7] G.S. Jiang, C.W. Shu, Efficient implementation of weighted ENO schemes, J. Comput. Phys. 126 (1996) 202–212.
[8] A. Harten, B. Engquist, S. Osher, S.R. Chakravarthy, Uniformly high order accurate essentially non-oscillatory schemes III, J. Comput. Phys. 71 (1987) 231–303.
[9] C. Hu, C.-W. Shu, Weighted essentially non-oscillatory schemes on triangular meshes, J. Comput. Phys. 150 (1999) 97–127.
[10] V.P. Kolgan, Application of the minimum-derivative principle in the construction of finite-difference schemes for numerical analysis of discontinuous solutions in gas dynamics, Uchenye Zapiski TsaGI [Sci. Notes of Central Inst. of Aerodynamics] 3 (6) (1972) 68–77 (in Russian).
[11] V.P. Kolgan, Finite-difference schemes for computation of three dimensional solutions of gas dynamics and calculation of a flow over a body under an angle of attack, Uchenye Zapiski TsaGI 6 (2) (1975) 1–6 (in Russian).
[12] X.D. Liu, S. Osher, T. Chan, Weighted essentially non-oscillatory schemes, J. Comput. Phys. 115 (1994) 200–212.
[13] V.V. Rusanov, Calculation of interaction of non-steady shock waves with obstacles, USSR J. Comput. Math. Phys. 1 (1961) 267–279.
[14] T. Schwartzkopff, C.D. Munz, E.F. Toro, ADER-2D: a high-order approach for linear hyperbolic systems in 2D, J. Sci. Comput. 17 (2002) 231–240.
[15] T. Schwartzkopff, M. Dumbser, C.D. Munz, Fast high order ADER schemes for linear hyperbolic equations, J. Comput. Phys. 197 (2004) 532–539.
[16] J. Shi, C. Hu, C.-W. Shu, A technique for treating negative weights in WENO schemes, J. Comput. Phys. 175 (2002) 108–127.

[17] N.N. Tilaeva, A generalization of the modified Godunov scheme to arbitrary unstructured meshes, Uchenye Zapiski TsaGI [Sci. Notes of Central Inst. of Aerodynamics] 17 (1986) 18–26 (in Russian).
[18] Y. Takakura, E.F. Toro, Arbitrarily accurate non-oscillatory schemes for a nonlinear conservation law, CFD J. 11 (N. 1) (2002) 7–18.
[19] V.A. Titarev, E.F. Toro, ADER: arbitrary high order Godunov approach, J. Sci. Comput. 17 (2002) 609–618.
[20] V.A. Titarev, E.F. Toro, High order ADER schemes for the scalar advection–reaction-diffusion equations, CFD J. 12 (1) (2003) 1–6.
[21] V.A. Titarev, E.F. Toro, Finite-volume WENO schemes for three-dimensional conservation laws, J. Comp. Physics (2004), to appear. Also Preprint NI03057-NPA. Isaac Newton Institute for Mathematical Sciences, University of Cambridge, UK, 2003, 33 pp.
[22] E.F. Toro, A weighted average flux method for hyperbolic conservation laws, Proc. Roy. Soc. London A 423 (1989) 401–418.
[23] E.F. Toro, Riemann Solvers and Numerical Methods for Fluid Dynamics, second ed., Springer, Berlin, 1999.
[24] E.F. Toro, Shock-Capturing Methods for Free-Surface Shallow Flows, Wiley, New York, 2001 314 pages.
[25] E.F. Toro, R.C. Millington, L.A.M. Nejad, Towards very high order Godunov schemes, in: E.F. Toro (Ed.), Godunov Methods. Theory and Applications, Edited Review, Kluwer Academic Publishers, Dordrecht, 2001, pp. 907–940.
[26] E.F. Toro, V.A. Titarev, Solution of the generalised Riemann problem for advection–reaction equations, Proc. Roy. Soc. London 458 (2018) (2002) 271–281.
[27] E.F. Toro, V.A. Titarev, TVD fluxes for the high-order ADER schemes, J. Sci. Comput., to appear. Also Preprint NI03011-NPA, Isaac Newton Institute for Mathematical Sciences, University of Cambridge, UK, 2003, 37 pp.
[28] B. van Leer, Towards the ultimate conservative difference scheme I: the quest for monotonicity, Lecture Notes Phys. 18 (1973) 163–168.
[29] B. van Leer, Towards the ultimate conservative difference scheme V: a second order sequel to Godunov' method, J. Comput. Phys. 32 (1979) 101–136.